PNAS Nexus

PNAS Nexus, 2023, **2**, 1–9
https://doi.org/10.1093/pnasnexus/pgac303
Advance access publication date: 6 January 2023
Research Report

A "grappling hook" interaction connects self-assembly and chaperone activity of Nucleophosmin 1

Mihkel Saluri[a], Axel Leppert[a,1], Genis Valentin Gese[c,1], Cagla Sahin[a,b], Dilraj Lama[a], Margit Kaldmäe[a], Gefei Chen[d], Arne Elofsson[e], Timothy M. Allison[f], Marie Arsenian-Henriksson[a], Jan Johansson[d], David P. Lane[a], B. Martin Hällberg[c,*] and Michael Landreh[a,*]

[a]Department of Microbiology, Tumor and Cell Biology, Karolinska Institutet – Biomedicum, Solnavägen 9, 171 65 Solna, Stockholm, Sweden
[b] Structural Biology and NMR laboratory and the Linderstrøm-Lang Centre for Protein Science, Department of Biology, University of Copenhagen,, Ole Maaløes vej 5, 2200 Copenhagen, Denmark.
[c]Department of Cell and Molecular Biology, Karolinska Institutet – Biomedicum, Solnavägen 9, 171 65 Solna, Stockholm, Sweden
[d]Department of Biosciences and Nutrition, Karolinska Institutet, 141 57 Huddinge,, Sweden
[e]Science for Life Laboratory and Department of Biochemistry and Biophysics, Stockholm University, 114 19 Stockholm, Sweden
[f] Biomolecular Interaction Centre, School of Physical and Chemical Sciences, University of Canterbury, Upper Riccarton, Christchurch 8041, New Zealand
*To whom correspondence should be addressed. Email: michael.landreh@ki.se or martin.hallberg@ki.se
Edited By: Binsen Li
Classification: Biological Sciences: Biophysics and Computational Biology.

Abstract

How the self-assembly of partially disordered proteins generates functional compartments in the cytoplasm and particularly in the nucleus is poorly understood. Nucleophosmin 1 (NPM1) is an abundant nucleolar protein that forms large oligomers and undergoes liquid–liquid phase separation by binding RNA or ribosomal proteins. It provides the scaffold for ribosome assembly but also prevents protein aggregation as part of the cellular stress response. Here, we use aggregation assays and native mass spectrometry (MS) to examine the relationship between the self-assembly and chaperone activity of NPM1. We find that oligomerization of full-length NPM1 modulates its ability to retard amyloid formation in vitro. Machine learning-based structure prediction and cryo-electron microscopy reveal fuzzy interactions between the acidic disordered region and the C-terminal nucleotide-binding domain, which cross-link NPM1 pentamers into partially disordered oligomers. The addition of basic peptides results in a tighter association within the oligomers, reducing their capacity to prevent amyloid formation. Together, our findings show that NPM1 uses a "grappling hook" mechanism to form a network-like structure that traps aggregation-prone proteins. Nucleolar proteins and RNAs simultaneously modulate the association strength and chaperone activity, suggesting a mechanism by which nucleolar composition regulates the chaperone activity of NPM1.

Keywords: native mass spectrometry, molecular chaperones, amyloid formation, membraneless organelles

Significance statement:

Membraneless organelles perform specific tasks inside the cell, yet it is unclear how assemblies of disordered proteins give rise to functional structures. A prominent example is the nucleolus, which prevents protein aggregation under stress and controls ribosome assembly. Here, we investigate the scaffold protein Nucleophosmin 1 (NPM1), which controls the liquid-like properties of the nucleolus. We find that NPM1 self-assembles through fuzzy interactions of its acidic tracts with its C-terminal chaperone domain. Ribosomal proteins and RNA tighten the association of NPM1 oligomers, blocking access to the C-terminus. Our study shows, how self-assembly and chaperone function can be controlled simultaneously by involving the same domain. This principle reveals a blueprint for the "structure—function"-based regulation of membraneless organelles.

Introduction

The nucleolus, the site of ribosome biogenesis in the nucleus, is a membraneless compartment that responds to changes in cellular growth rate, metabolic activity, and stress (1). Its dynamic nature allows a constant exchange of proteins and nucleotides with the surrounding nucleus and the cytoplasm. For example, the nucleolus sequesters $p14^{ARF}$ and its binding partner human double minute 2 homolog (HDM2), which otherwise ubiquitinylates the tumor suppressor p53 to allow cell cycle progression (2). Its ability to recruit and release proteins has been attributed to the fact that nucleolar assembly is driven by liquid–liquid phase separation (LLPS) of a highly enriched subset of nucleolar proteins (3). By exhibiting different phase-separating properties, these proteins account for the coexistence of nucleolar regions with distinct functions (4). Nucleophosmin 1 (NPM1, also known as B23) is the main component of the outermost nucleolar phase, the granular com-

Competing Interests: The authors declare no competing interests
[1]A.L. and G.V.G. contributed equally
Received: October 5, 2022. **Accepted:** January 5, 2023

ponent, where ribosomes are assembled. Mutations in NPM1 are commonly associated with acute myeloid leukemia (AML) (5). It is the main nucleolar interaction partner for the $p14^{ARF}$ tumor suppressor and the c-MYC oncoprotein, and knockdown experiments have identified NPM1 as a promising target for cancer therapy (6, 7).

NPM1 has a modular structure with folded N-terminal and C-terminal domains (NTD, residues 1 to 120, and CTD, residues 240 to 294) linked by an intrinsically disordered region (IDR, residues 120 to 240) (Fig. 1a). The N-terminal domain adopts a β-sheet sandwich fold and assembles into pentamers that can form end-to-end decamers (8). The NTD and IDR contain three highly acidic poly-D/E stretches (A1, A2, and A3), as well as two regions with predominantly basic residues (B1 and B2) (9). The CTD is a nucleotide-binding domain composed of thee α-helices and is the site of AML-related mutations, which result in removal of a nucleolar localization signal (10). Full-length (FL) NPM1 self-assembles into large oligomers in isolation (9, 11) and in cancer cells (12). The addition of polyanionic or polycationic molecules, such as basic peptides or RNA, induce LLPS through heterotypic interactions with the opposing charges on FL NPM1 (9). The isolated NTD can also undergo LLPS by binding basic peptides via its acidic A1 region (13). In addition, oligomeric NPM1 engages in homotypic interactions through contacts between its charged regions, which can give rise to LLPS under crowding conditions and are modulated by ionic strength (9, 14).

Besides its role as a nucleolar scaffold, NPM1 has a chaperone activity in vitro and effectively prevents the aggregation of denatured proteins (15). Strikingly, the nuclear proteome is enriched in disordered and aggregation-prone proteins (16). The nucleolus can sequester misfolded proteins during cellular stress and turn them over to HSP70 for refolding (17). It also stores protein aggregates in amyloid bodies that may function as "nucleolar detention centers" for potentially toxic aggregates (18). In cells, NPM1 colocalizes with misfolded proteins and amyloids, suggesting that it functions as a chaperone during cellular stress (17) (Fig. 1b). Importantly, deletion of individual domains of NPM1 reduces its ability to counteract thermal denaturation of proteins (11). Together, these findings raise the possibility that the chaperone function of NPM1 in the nucleolus is related to its self-assembly properties.

Results

Full-length NPM1 and its CTD display differential chaperone activity toward amyloid formation

Previous studies have established the ability of FL NPM1 to protect globular proteins from thermal and chemical denaturation (11, 15). However, several amyloidogenic proteins are targeted to the nucleus (19), and NPM1 associates with nucleolar amyloid aggregates in vivo (17). We, therefore, tested the ability of NPM1 to prevent the aggregation of amyloid-β_{1-42} ($A\beta_{42}$), which has been found in the nuclei of neurons from Alzheimer's disease patients and is considered a model for amyloid formation (20, 21). It has to be noted that $A\beta_{42}$ has no confirmed nucleolar localization and is not likely to be a physiological target of NPM1, but is widely used as a model system to study the generic anti-amyloid activity of chaperone proteins (22, 23).

Briefly, we incubated 3 μM $A\beta_{42}$ with 0 to 6 μM NPM1 in the presence of the amyloid-specific dye Thioflavin T (ThT) and monitored fibril formation through the increase in fluorescence intensity (Fig. 1c). The addition of NPM1 delayed the half-time of fibrillation in a concentration-dependent manner, with the most pronounced effect at an NPM1 : $A\beta_{42}$ ratio of 1:1 (Fig. 1c). The end-point fluorescence intensity was in all cases comparable to that of $A\beta_{42}$ alone (Fig. S1a). Interestingly, NPM1 does not appear to specifically affect only primary or secondary nucleation, or fibril elongation, but rather all of these processes. Together, these observations suggest that NPM1 efficiently retards the amyloid assembly processes. To identify which parts of the modular NPM1 structure are responsible for delaying $A\beta_{42}$ aggregation, we designed truncated variants: $NPM1_{120}$, which contains only the NTD with the A1 tract, $NPM1_{188}$, which includes the NTD and the acidic tracts A1-3, $NPM1_{240}$, which encompasses the NTD and the entire IDR, and $NPM1_{240\text{-}294}$, which represents the isolated CTD (Fig. 1d). We then tested the effects of all NPM1 variants on $A\beta_{42}$ fibrillation under the same conditions as for FL NPM1 and determined the half-time of $A\beta_{42}$ fibrillation ($t_{1/2}$). Plotting the $A\beta_{42}$ $t_{1/2}$ in the presence of FL NPM1, $NPM1_{120}$, $NPM1_{188}$, and $NPM1_{240}$ shows that full-length NPM1 affects $A\beta_{42}$ aggregation in a dose-dependent manner, whereas the C-terminally truncated variants have only minor effects (Fig. 1e). $NPM_{240\text{-}294}$, i.e., the isolated CTD, a dose-dependent delay in ThT fluorescence at a concentration of 0.3 μM, and additionally resulted in a strong suppression of ThT fluorescence when the concentration was raised further (Fig. 1f). Strikingly, none of the other NPM1 constructs resulted in a similar decrease in end-point fluorescence (Fig. S1a). In agreement with the ThT data, electron microscopy showed no fibrils in the presence of the CTD at the reaction end-point. (Fig. S1b). Together, these observations indicate that the ability of NPM1 to delay fibril formation is related to its CTD but appears to be reduced in the FL protein. To test whether NTD and CTD work synergistically to delay $A\beta_{42}$ fibrillation, we incubated $A\beta_{42}$ with 3 μM $NPM1_{240}$ and 3 μM $NPM1_{240\text{-}294}$. However, the combined effect of both NPM1 parts on fibril formation was far less pronounced than for FL NPM1 at the same concentration (Fig. S1b). This finding shows that the chaperone activity of the CTD is reduced in the presence of the NTD, but the effect is less pronounced when the NTD is part of the same polypeptide than when it is added in trans. These observations imply that inter-domain interactions in the FL protein regulate its chaperone activity towards $A\beta_{42}$.

A covalent link between NTD and CTD is required for NPM1 self-assembly

To better understand the relationship between chaperone activity and interdomain interactions, we turned to native mass spectrometry (MS). Here, intact protein complexes are transferred from the solution to the gas phase using soft electrospray ionization (nESI). Since noncovalent interactions can be preserved during mass measurements, we can obtain information about the oligomeric states of protein complexes in solution (24, 25). In combination with collision-induced dissociation, where the intact complexes are subjected to high-energy collisions with an inert buffer gas inside the mass spectrometer, we can determine their composition. By comparing the collision voltages required to dissociate protein interactions, we can furthermore assess their relative stabilities (26) (Fig. 2a).

First, we subjected FL NPM1 to native MS analysis (Fig. 2b). Under gentle MS conditions (collision voltage 25 V), we could only detect an unresolvable "hump" that is characteristic of large assemblies with no well-defined stoichiometry (27). When raising the collision voltage to 75 V, we obtained well-resolved peaks corresponding in mass to monomers, dimers, trimers, and pentamers of FL NPM1. We did not detect higher oligomeric states than pentamers and consider that the monomers, dimers, and trimers

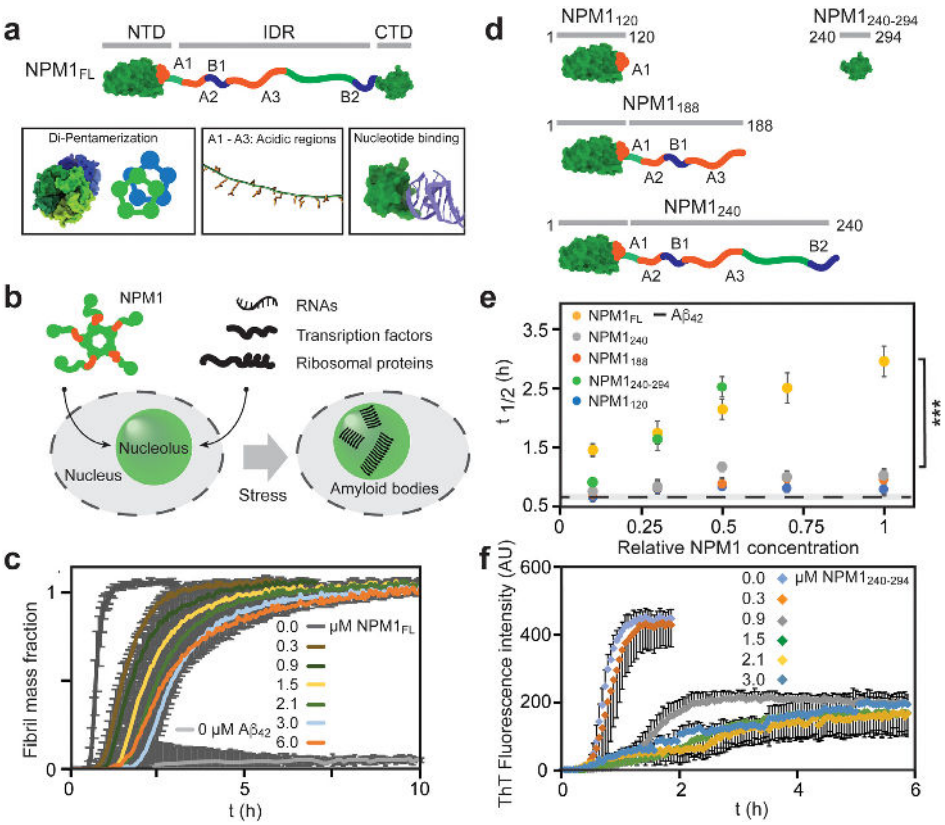

Fig. 1. NPM1 delays Aβ_{42} aggregation. (a) NPM1 has a modular architecture, composed of a folded N-terminal pentamerization domain (NTD, residues 1 to 120), an intrinsically disordered region (IDR, residues 120 to 240) containing three acidic and two basic tracts (A1-3 and B1 and 2, respectively), and a C-terminal nucleotide-binding domain (CTD, residues 240 to 294). The NTD and the CTD are rendered based on PDB IDs 2P1B and 2VXD, respectively. (b) NPM1 pentamers associate with RNA, basic transcription factors, and ribosomal proteins to form the granular component of the nucleolus. Cellular stress induces the formation of nucleolar amyloid bodies. (c) The presence of increasing amounts of NPM1 shows that NPM1 delays the onset and the elongation of fibrillation, as judged by ThT fluorescence. Error bars indicate the SD of $n = 4$ experiments. (d) Truncated variants of NPM1 used in this study: $NPM1_{120}$ encompasses the NTD. $NPM1_{188}$ the NTD and the acidic regions of the IDR, $NPM1_{240}$ the NTD and the entire IDR and $NPM1_{240\text{-}294}$ only the CTD. (e) Fibrillation half-times ($t_{1/2}$) of Aβ_{42} in the presence of 0 to 3 μM of NPM1 variants shows that only FL NPM1 and $NPM1_{240\text{-}294}$, but no other truncated variants, affects fibrillation. The $t_{1/2}$ of Aβ_{42} alone is shown as a dashed line. Error bars indicate the SD of $n = 4$ experiments. A one-way ANOVA was used to test for the overall significant difference between groups before running pairwise *t*-tests with Bonferroni correction. Asterisks indicate significant differences ($P < 0.001$). (f) ThT fluorescence curves of Aβ_{42} in the presence of 0 to 3 μM $NPM1_{240\text{-}294}$ show a dose-dependent delay in fibrillation and a decrease in fluorescence intensity. Error bars indicate the SD of $n = 4$ experiments.

likely are dissociation products. These findings indicate that FL NPM1 pentamers assemble into large oligomers, in agreement with previous reports (9, 11, 12). Next, we analyzed, oligomerization of the truncation variants. NPM_{120} yielded well-resolved spectra at a collision voltage of 50 V. Strikingly, we observed a broad range of oligomeric states, ranging from 5 to 50 subunits, but always in multiples of five, suggesting that the NTD pentamers can assemble into polymers (Fig. 2b). The charge state distribution of a protein ion is dependent on its surface area (28, 29), allowing structural information to be extracted. Plotting the average charge of each oligomeric state as a function of its molecular weight results in a correlation, which closely follows the trend expected for globular proteins (Fig. S2a). The crystal structure of $NPM1_{120}$ shows side-by-side and end-to-end association of NTD pentamers in a crystal lattice via salt bridges (Fig. S2b), which leads us to speculate that crystal-like interactions drive multimerization of the NTDs. MS analysis of $NPM1_{188}$, which includes the IDR region with acidic tracts A2 and A3 required moderately higher collision voltages (75 V). The resulting mass spectra show pentamers and decamers, but not any higher oligomeric states, indicating that the IDR disrupts the self-association propensity of the isolated NTDs. Native MS analysis of $NPM1_{240}$, which includes the entire IDR, yielded essentially the same oligomeric state as $NPM1_{188}$ but with a slightly lower amount of decamers. Last, we also examined the isolated CTD, $NPM1_{240\text{-}294}$. Native mass spectra show monomeric protein, with no sign of higher oligomerization besides traces of dimers (Fig. 2d). Taken together, native MS reveals three types of NPM1 oligomerization, which are governed by the three domains: (1) the isolated NTD forms pentamers that self-assemble into ordered multimers; (2) the IDR disrupts these NTD multimers, yielding pentameric protein; (3) including the CTD induces the formation of large oligomers which can be dissociated into pentamers and pentamer fragments. We conclude that the formation of higher NPM1 oligomers requires full-length protein, suggesting direct interactions involving the CTD.

NPM1 pentamers connect via their CTDs

The observations from MS suggest that the CTD is involved in the higher oligomerization of NPM1. We therefore used fluorescence spectroscopy to test for interactions between the CTD and other regions of the protein. Importantly, the only two tryptophane residues in NPM1 are in the CTD, which allowed us to use intrinsic fluorescence to probe its interaction in solution. We found that

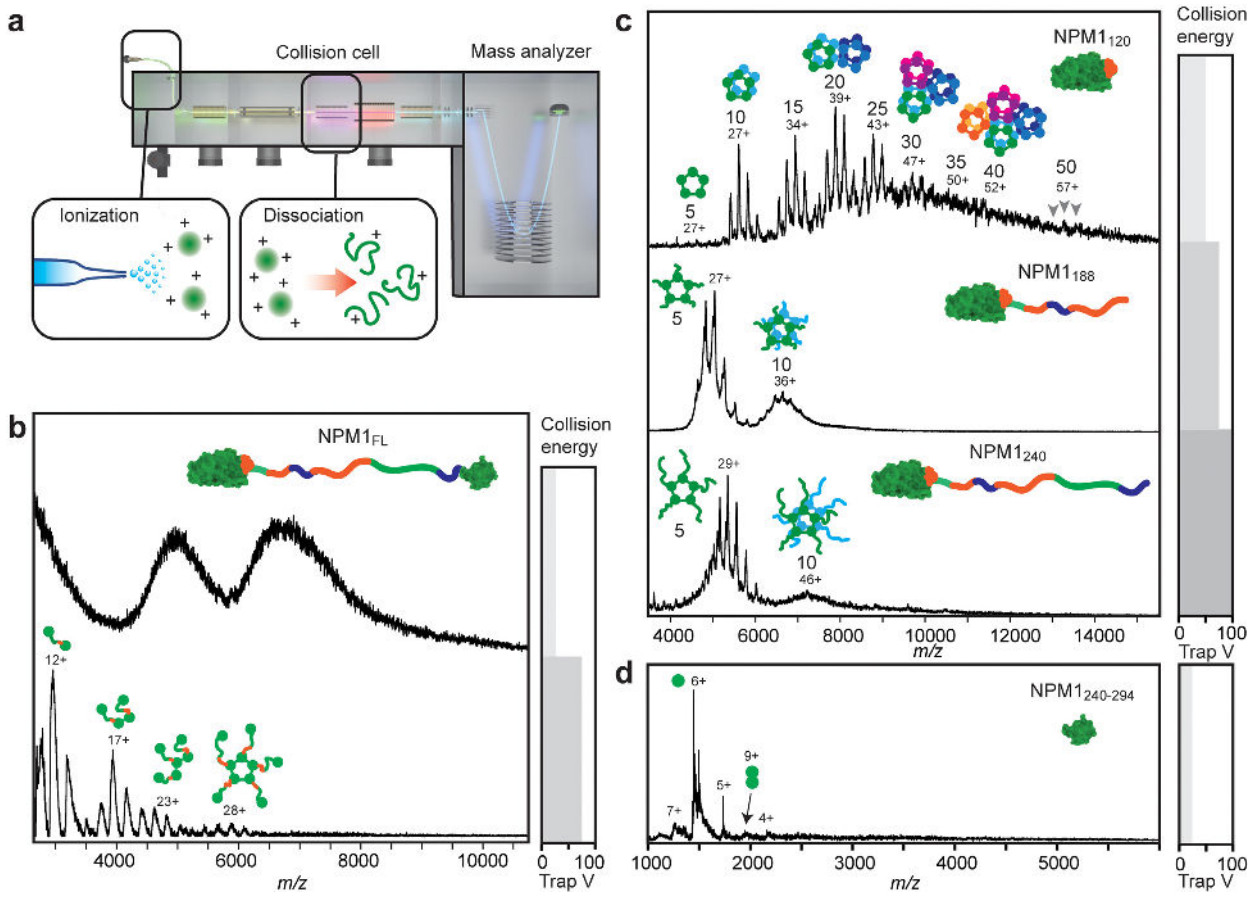

Fig. 2. Native MS shows that higher oligomerization is specific for $NPM1_{FL}$. (a) A schematic illustration of the native MS experiment, using collision-induced dissociation in the collision cell of the MS instrument. The illustration has been adapted from (43). (b) The native mass spectra of NPM1 at low collision energy show unresolved baseline humps, indicating large oligomers (top). Increasing the collision voltage releases NPM1 monomers, dimers, trimers, and pentamers (bottom). (c) The mass spectra of $NPM1_{120}$ show a range of oligomeric states composed of multiples of five subunits, as indicated. $NPM1_{188}$ and $NPM1_{240}$ form predominantly pentamers and minor decamer populations. (d) The isolated CTD ($NPM1_{240\text{-}294}$) exists nearly exclusively as monomers. The respective collision voltage at which each spectrum was obtained is indicated on the right.

the addition of quadruplex DNA, a high-affinity ligand for the CTD (30), quenches the intrinsic fluorescence of $NPM1_{240\text{-}294}$, indicating binding (Fig. 3a). We then tested whether the N-terminal region of NPM1 affected tryptophane fluorescence. The addition of $NPM1_{120}$ resulted in a mild decrease in fluorescence intensity, whereas the addition of $NPM1_{240}$ had a more pronounced effect. The presence of both DNA and $NPM1_{240}$ gave an intermediate fluorescence reduction. Taken together, the change in tryptophane fluorescence suggests a direct association between $NPM1_{240\text{-}294}$ and $NPM1_{240}$, which is impacted by the presence of DNA.

To better understand how the CTD associates with other parts of NPM1, we turned to cryo-electron microscopy (cryo-EM). Using physiological conditions (pH 7.5 and 150 mM NaCl), we obtained electron density maps that allowed a reconstruction of the NTD with a resolution of 2.6 Å (Fig. S3, Table S1). Comparison to the crystal structure revealed a virtually identical fold, including sidechain orientations, except for the loop covering residues 34 to 39, which makes up the A1 tract. In the X-ray structure, it is stabilized via crystal contacts with the neighboring pentamer (Fig. S2). In the cryo-EM density maps, the loop is too flexible for a confident reconstruction, suggesting that not only the A2 and A3 tracts but even the A1 tract in the NTD is disordered (Fig. 3b). Free CTDs attached to the disordered linker are too small (less than 9 kDa) to be resolved on their own. Interestingly, we obtained two distinct 3D classes, one with an additional density above the acidic side of the pentamer, off-center from central cavity (Fig. 3c). Strikingly, nearly all particles in this class had another NTD pentamer in the proximity (Fig. S4a). Particles in the second class, on the other hand, did not show the extra density and had less nearby particles (Fig. 3d and Fig. S4b). The extra density is connected to the pentamer via the A2 tract of a single NTD and can therefore not be attributed to the disordered regions of each protomer (Fig. S4c). We speculated that the density could stem from interactions involving the CTD.

To test this possibility, we turned to AlphaFold (AF), a neuronal network that can predict the 3D structures of protein complexes with an accuracy that rivals experimentally determined structures (31, 32). Capitalizing on the ability to AF to dock short, disordered peptide segments with high confidence (33), we divided the IDR of NPM1 into peptides of 20 amino acids with a 10-residue overlap and predicted possible complexes with the CTD (Fig. 3e, Fig. S5). We then calculated the binding energies for the top-scoring complex for each peptide. We found that peptides covering the acidic tracts A2 or A3 exhibited weakly favorable interactions due to charge contacts with the basic residues in the CTD. Placement of the top-scoring complex between the CTD and the A2 tract into the EM map showed a good agreement between the unassigned density, the helical acidic region of the IDR, and the approximate location of the CTD (Fig. S4d). Considering the flexibility of the IDR,

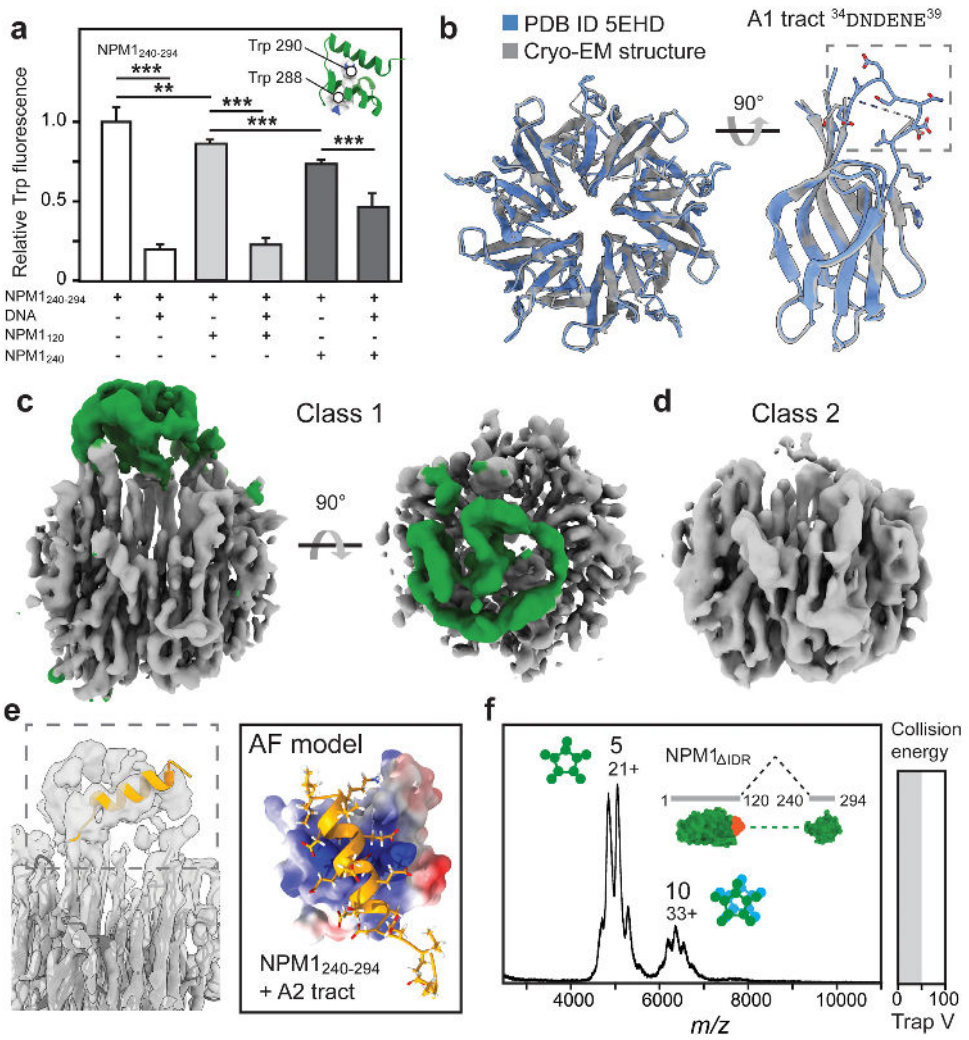

Fig. 3. An NTD–CTD interaction in FL NPM1. (a) The fluorescence of tryptophane residues 288 and 290 in $NPM_{240-294}$ is quenched by the addition of equimolar amounts of DNA or NPM_{240}, and to a lesser extent by NPM_{120}. In the presence of DNA and NPM_{240}, intermediate quenching is observed. Error bars indicate the SD of $n = 6$ repeats. One-way ANOVA was used to test for the overall significant difference between groups before running pairwise t-tests with Bonferroni correction. Asterisk indicates significance (** $P < 0.01$ and *** $P < 0.001$). (b) The cryo-EM reconstruction of the NTD (gray) shows virtually no deviations from the crystal structure (PDB ID 5EHD, blue), except for the A1 tract (residues 34 to 39), which could not be modeled based on the density map. (c) The cryo-EM density map for FL NPM1 reveals an additional asymmetric density (green) above the NTD pentamer (gray). (d) A second 3D class with fewer neighboring particles does not show the additional density. (e) The helical A2 tract (orange) appears as a diffuse density in the EM map. AF predicts a complex between the helical A2 tract (orange) and the basic CTD (rendered as an electrostatic surface). (f) Native MS of the $NPM_{\Delta IDR}$ variant lacking the disordered region between residues 120 and 240 reveals pentamers and a small fraction of decamers but no higher oligomers.

the CTD would be unlikely to occupy a more specific orientation, giving rise to a more diffuse density than the pentameric NTD.

We then confirmed interaction between the disordered region and CTD by recording mass spectra of $NPM1_{188}$ and $NPM1_{240-294}$. We observed unresolvable peaks and a shift to the higher m/z region for $NPM1_{188}$, indicating binding of the CTD with a mixed stoichiometry (Fig. S6a). Next, we designed a short NPM1 variant, $NPM1_{\Delta IDR}$, in which NTD and CTD are linked without the IDR (Fig. 3f). Native MS analysis of $NPM1_{\Delta IDR}$ revealed almost exclusively pentameric protein and a small decamer population, irrespective of collision voltage (Fig. 3f). This result demonstrates that removing the IDR prevents higher oligomerization of NPM1 pentamers. Taken together, fluorescence spectroscopy, AF, cryo-EM, and MS suggest that the CTD engages in weak, "fuzzy" interactions with the disordered region of neighboring pentamers. The IDR and CTD can be viewed as a "grappling hook" that links NPM1 into large oligomers.

Since the interactions between CTD and IDR affect nucleotide binding to NPM1, we recorded mass spectra of FL NPM1 in the presence of equimolar amounts of tRNA, which binds to NPM1 and is more homogeneous than rRNA and thus easier to detect by MS. We found that tRNA completely abolishes the NPM1 signal in MS even at high collision voltages (Fig. S6b), consistent with tRNA cross-linking the NPM1 pentamers into oligomers that are too stable for gas-phase dissociation. We also considered AML mutations that disrupt the third helix of the CTD and asked whether they may impact self-assembly. We purified an NPM1 variant with a mutation at the C-terminus ($NPM1_{AML}$) in which the last seven residues (WQWRKSL) are exchanged for an 11-residue sequence lacking the nucleolar localization signal (CLAVEEVSLRK) and recorded mass spectra under native conditions. Strikingly, we

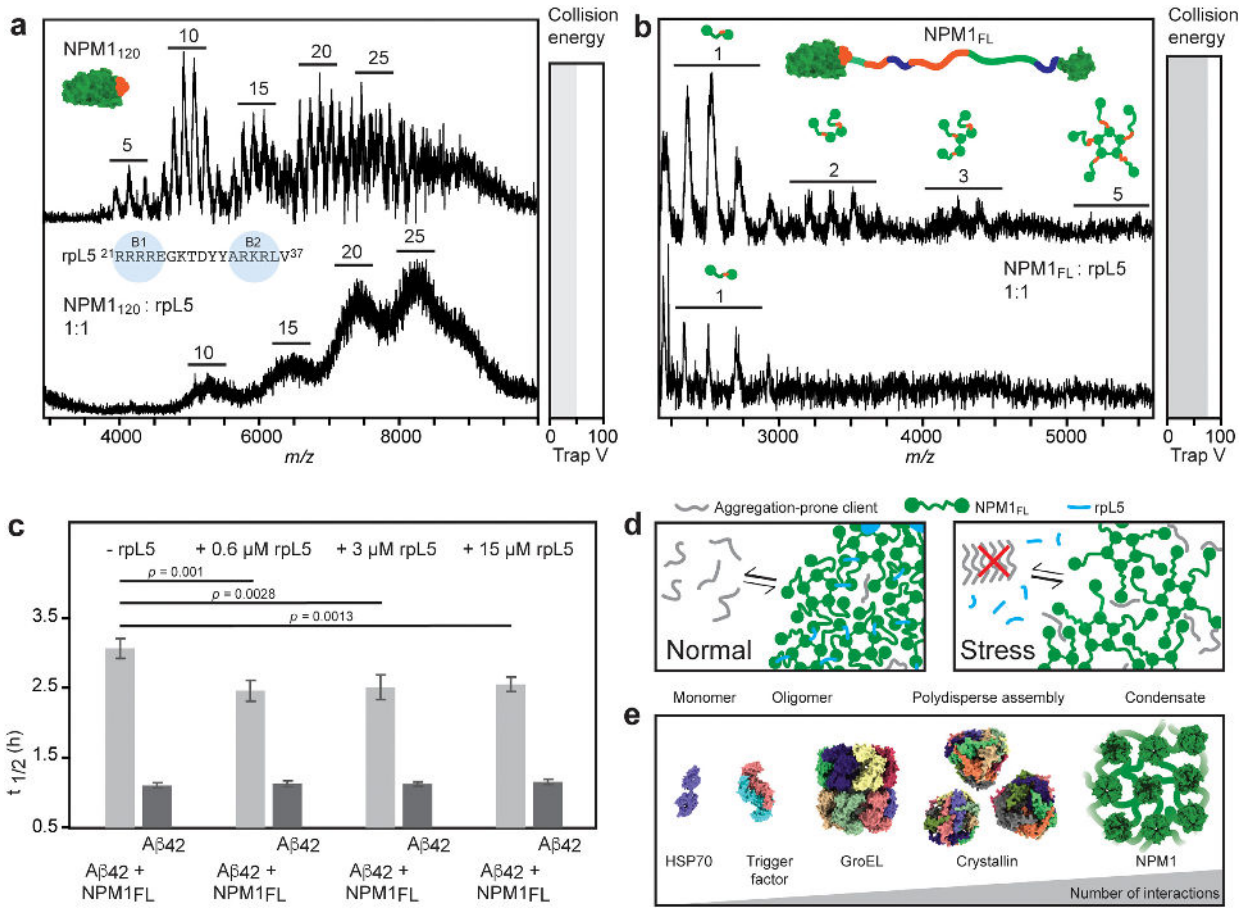

Fig. 4. Modulating NPM1 self-assembly impacts its chaperone activity. (a) Residues 21 to 37 of rpL5 contain two basic motifs (B1 and B2). The native mass spectra of $NPM1_{120}$ show peak broadening and a shift to higher oligomeric states in the presence of $rpL5_{21\text{-}37}$. (b) FL NPM1 assemblies formed with $rpL5_{21\text{-}37}$ cannot be dissociated by collisional activation, as judged by the low abundance of monomers and the absence of dimers, trimers, or pentamers in the mass spectra. (c) Comparing the $t_{1/2}$ for fibril formation as judged by ThT fluorescence shows that $rpL5_{21\text{-}37}$ alone does not affect $A\beta_{42}$ aggregation, whereas $rpL5_{21\text{-}37}$ reduces the ability of NPM1 to delay $A\beta_{42}$ fibrillation. Error bars indicate the SD of $n = 4$ repeats. Significance was calculated using a Student's *t*-test for paired samples with equal variance. (d) Proposed connection between chaperone activity and self-assembly of NPM1. Under normal conditions, NPM1 (green) and basic proteins (blue) such as rpL5 form a tight nucleolar network. Under stress, rpL5 is released from the nucleolus, loosening up the NPM1 network, which enables NPM1 to sequester and chaperone amyloidogenic client proteins (gray). (e) Oligomerization and chaperones. Chaperone stoichiometries range from monomers (HSP70) to polydisperse oligomers (α-crystallin B). Chaperone activity of NPM1, on the other hand, involves the formation of large assemblies without defined stoichiometry.

did not observe a pronounced difference between FL NPM1 and $NPM1_{AML}$ (Fig. S6c). We conclude that the AML variants do not exhibit altered self-assembly properties, and that its oncogenic potential can therefore be attributed to loss of the nucleolar localization signal in helix 3.

Nucleolar components modulate NPM1 self-assembly and chaperone activity

Having established that CTD interactions mediate NPM1 self-assembly, we then asked whether the same interactions affect its ability to delay $A\beta_{42}$ fibrillation. It is well established that NPM1 can undergo LLPS through heterotypic interactions with RNA or basic peptides located in the nucleolus. Peptides such as residues 21 to 37 of ribosomal protein L5 (rpL5) or residues 299 to 326 of SURF6, which both contain multiple arginine-rich motifs, bind to the A1 tract of NPM1 and induce LLPS (13). The same type of interaction has been found to mediate sequestration of $p14^{ARF}$ by nucleolar NPM1 (34, 35). We speculated that such interactions would compete with higher oligomerization via the CTD.

To test this possibility, we selected $rpL5_{21\text{-}37}$, a short peptide with two basic motifs and whose association with NPM1 has been investigated in detail (Fig. 4a) (13, 36). The AF model shows binding of the second basic motif of $rpL5_{21\text{-}37}$ to the acidic A1 groove on the NTD, while the first basic motif is extended away from the protein, making it accessible for charge interactions with another NTD (Figure S7c). This model, in agreement with previous reports (13), thus suggests that $rpL5_{21\text{-}37}$ cross-links acidic regions in NPM1. We monitored the effect of $rpL5_{21\text{-}37}$ on NPM1 self-assembly by incubating FL NPM1 for 60 min at room temperature in the absence or the presence of increasing concentrations of the peptide and following the accumulation of sedimented macroscopic assemblies by light microscopy (Fig. S7a). After incubation of NPM1 alone, we detected a small number of spherical aggregates, which may be related LLPS of NPM1 in the presence of trace amounts of nucleotides not detectable by MS. Addition of $rpL5_{21\text{-}37}$ at a ratio of 1:10 caused a notable increase in assembly size and fusion into larger, amorphous structures. After 60 min incubation at a 10-fold excess of $rpL5_{21\text{-}37}$, exclusively amorphous assemblies were observed. Assemblies formed in the presence of $rpL5_{21\text{-}37}$ stained positively for the phase separation-specific DroProbe dye (Fig. S7b) (37). Since $rpL5_{21\text{-}37}$ can induce the assembly of both FL NPM1 as well as the isolated NTD (13), we recorded the mass spectra of

$NPM1_{120}$ in the presence of $rpL5_{21-37}$ (Fig. 4a). We observed significant peak broadening, indicating binding of the 2.2 kDa peptide to $NPM1_{120}$ oligomers, as well as a shift from predominantly decamers to oligomers composed of ≥25 subunits. Next, we subjected complexes between FL NPM1 and $rpL5_{21-37}$ to MS analysis. Notably, we did not detect pentamers or their fragments upon collisional activation, but only trace amounts of monomers (Fig. 4b). Together, the insights from MS suggest that $rpL5_{21-37}$ binding increases the size and stability of NPM1 oligomers by cross-linking acidic tracts. Importantly, these oligomers have a considerably closer association between NTD pentamers than those formed by interactions with the CTD, due to the short length of the $rpL5_{21-37}$ peptide.

The fact that the $rpL5_{21-37}$ peptide modulates higher oligomerization of NPM1 enabled us to test the impact of self-assembly on chaperone activity. We, therefore, performed aggregation assays with $A\beta_{42}$ and FL NPM1 in the presence of increasing amounts of $rpL5_{21-37}$ (Fig. 4c). Although $rpL5_{21-37}$ alone had no effect on $A\beta_{42}$ fibrillation, it significantly reduced the ability of NPM1 to delay the formation of ThT-positive aggregates (Fig. 4c, Fig. S7d). Interestingly, the effect was observed already at a 5-fold excess of NPM1, corresponding to one $rpL5_{21-37}$ per pentamer. These data suggest that inducing a tighter and more complete association of NPM1 subunits through basic nucleolar peptides reduces its chaperone activity. To investigate whether the observations for $rpL5_{21-37}$ represent a general mechanism, we also tested the $SURF6_{299-326}$ peptide, which encompasses basic tract 4 of SURF6 and induces LLPS of NPM1 (13, 38). AF models indicate a binding mode similar to that of $rpL5_{21-37}$ (Fig. S7f), in good agreement with their comparable effects on NPM1 assembly (13, 38). Aggregation assays showed that $SURF6_{299-326}$ alone has no impact on $A\beta_{42}$ fibrillation but reduces the efficiency of FL NPM1 chaperoning to a similar extent as $rpL5_{21-37}$ (Fig. S7e, g). We conclude that proteins or peptides with multiple basic motifs cross-link NPM1 oligomers, which reduces their ability to delay fibril formation in vitro.

Discussion

The nucleolar scaffold protein NPM1 controls p53-dependent tumor suppression by sequestering aggregation-prone transcription factors, including $p14^{ARF}$ and c-MYC (7) and is implicated in the formation of amyloid bodies under stress conditions (18). In this study, we have investigated the basis of NPM1 self-assembly and how it relates to its ability to prevent amyloid formation in vitro. The CTD of NPM1 can delay fibrillation of the model amyloid $A\beta_{42}$, yet this chaperone activity is modulated by NPM1 self-assembly. Using a combination of native MS, machine learning, and cryo-EM, we show that direct interactions between CTD and the acidic IDR in NPM1 induce the formation of an NPM1 network and thus reduce its ability to delay $A\beta_{42}$ aggregation. Our findings imply that NPM1 pentamers are linked by their CTDs and IDRs, although additional interactions of the CTDs with the acidic NTDs cannot be excluded, as AF models of 29 homologs from the Pfam with identical domain architecture as NPM1 with sequence identities below 50% show clustering of the CTDs around the acidic side of the NTDs (Fig. S8). The length of the IDR (approximately 120 residues) leaves considerable space between the NPM1 pentamers, creating flexible compartments lined with acidic and some basic residues. Previous studies have suggested diffuse interactions between the acidic and basic tracts in oligomers (13), which could regulate the degree of compaction of the NPM1 network. The addition of basic peptides such as rpL5 or SURF6 cross-links the acidic NTDs and potentially the other acidic tracts, to constrict the network, in line with the induction of LLPS of NPM1 by polycations (9, 13) (Fig. 4d).

Our findings raise the question of how exactly NPM1 oligomers interact with unfolded or aggregation-prone clients. The observation that NPM1 does not seem to specifically inhibit primary or secondary nucleation or fibril elongation but rather affects all these events indicates that NPM1 works by partially sequestering $A\beta_{42}$. We speculate that a fraction of the $A\beta_{42}$ species are trapped in the NPM1 network and released on an equilibrium basis. Importantly, $A\beta_{42}$ has not been identified as a client of NPM1 in vivo and does not include highly charged motifs that would promote recruitment into the NPM1 network via interactions with basic or acidic tracts. The fact that the chaperone activity of the CTD is higher than that of FL NPM1 suggests that $A\beta_{42}$ can interact with free CTDs, and that this interaction is reduced when the CTDs instead bind to IDRs of neighboring NPM1 pentamers. The artificial amyloid β17, which shares some characteristics with $A\beta_{42}$, colocalizes with NPM1 in cells (17), underscoring the possibility that NPM1 may bind a wider range of aggregation-prone sequences. Importantly, the isolated CTD does not prevent aggregation of denatured globular proteins, which instead requires FL NPM1 (11, 15). These differences indicate different mechanisms for chaperoning unfolded proteins and amyloidogenic peptides, a distinction that has been reported for other chaperone systems (23, 39, 40). Unfolded proteins expose hydrophobic as well as charged patches, which may drive their recruitment into NPM1 oligomers. The fact that the nucleolus does not actively promote refolding but holds unfolded proteins before transferring them to the HSP70 network supports this concept (17).

We hypothesize, based on our findings, that changes in nucleolar composition could balance the ability of the NPM1 scaffold to chaperone unfolded proteins or amyloids. Basic proteins, including rpL5 and $p14^{ARF}$, mediate tight connections between the NPM1 pentamers but are released under stress conditions. The resulting loosening of the NPM1 network serves to activate the chaperone function of NPM1, in line with its role as safeguard against stress-induced protein aggregation (Fig. 4d). In this context, NPM1 may be viewed as an extreme case of a polydisperse chaperone (Fig. 4e).

Considering the limited physiological relevance of the NPM1-$A\beta_{42}$ model system, we speculate that other proteins with a similar combination of charged regions, disordered regions, and oligomerization potential may exert a similar anti-amyloid activity. Such a protein has recently been identified as a noncanonical chaperone: the death-domain associated protein (DAXX) contains a folded N-terminal domain as well as a disordered region with poly-glutamate and poly-aspartate stretches and undergoes LLPS through interactions with p62 (41). DAXX can prevent $A\beta_{42}$ fibrillation as well as the aggregation of heat-denatured proteins and associates with p53 to ensure correct folding (22). It furthermore controls nucleolar integrity (42), raising the possibility that poly-D/E proteins constitute a class of chaperones that incorporate into nucleolar condensates. Identifying the physiological targets of these chaperones and which properties of poly-D/E proteins they recognize will be an important step toward understanding their biological function.

Although our study clearly shows that direct interactions involving the CTD modulate the chaperone activity of NPM1, it has some limitations, as it does not address the possibility of conformational changes in the disordered regions. Specifically, the experimental approach used here (cryo-EM, AF, and native MS) is best-suited for detecting complexes between folded domains For example, the density map outside of the NTD is too diffuse to allow any unambiguous reconstructions, and we could not ob-

serve by EM binding of the CTD to IDR further away from the NTD. Similarly, AF does not reliably predict the preferred conformations of disordered regions. We can infer some insights into the structure of the disordered region, e.g., from the absence of unassigned densities outside of the NTD complexes and the fact that $NPM1_{\Delta IDR}$ does not assemble, but we could not obtain atomistic insights into complexes between the CTD and FL NPM1. More broadly, the self-assembly of NPM1 is affected by multiple types of "fuzzy" interactions, including with polyanions, polycations, and molecular crowders (9), but we cannot independently assess their contributions to NPM1 chaperone activity within the scope of this study. Our results indicate that RNA and basic peptides increase the stability of NPM1 oligomers, but do not reveal whether this effect is related to phase separation of NPM1. For example, we observe a shift to larger oligomers of NPM_{120} in the presence of $rpL5_{12\text{-}37}$. However, the isolated NTD does not undergo phase separation with $rpL5_{12\text{-}37}$ unless the disordered A2 tract is included (13), which hints at a need for flexible connections between the protomers for LLPS to occur. Similarly, RNA molecules could increase the distance between NTD pentamers and thus modulate the fluidity of the assembly. Further studies are therefore needed to assess the specific role(s) of LLPS in nucleolar chaperoning.

Materials and Methods

The density maps for the N-terminal region ("CryoEM structure of the human Nucleophosmin 1 core") and for the two selected 3D classes have been deposited in the EMDB (EMD-15,606). The refined atomic coordinates for the NPM1 core have been deposited in the PDB with (code 8AS5). Full materials and methods are described in the Supplementary Material file.

Acknowledgments

The authors extend special thanks to Sergej Masich and access to the KI 3D-EM facility. ML gratefully acknowledges technical support from MS Vision, NL. This manuscript was posted on a preprint: https://doi.org/10.1101/2022.09.29.510028

Supplementary Material

Supplementary material is available at *PNAS Nexus* online.

Funding

M.L. is supported by a KI faculty-funded career position, a KI-Cancer Blue Sky grant, a Cancerfonden Project grant (19 0480), and a VR Starting Grant (2019–01961). A.L. is supported by the Olle Engkvist Foundation (to M.L.), and C.S. is supported by a Novo Nordisk Foundation Postdoctoral Fellowship (NNF19OC0055700). D.P.L. is supported by a Swedish Research Council grant for internationally recruited scientists (2013–08807). A.E. is supported by the Swedish Research Council for Natural Science, grant No. VR-2016–06301, the Swedish E-Science Research Centre, and the Knut and Alice Wallenberg Foundation. Computational resources: Swedish National Infrastructure for Computing, grants: SNIC 2021/5–297, SNIC 2021/6–197, and Berzelius-2021–29.

Authors' Contributions

M.S. and M.L. designed the study with input from T.M.A., M.A.H., D.P.L., and J.J. M.S. and M.K. produced NPM1 variants, and G.C. produced Ab42. M.S. and A.L. performed aggregation assays. M.S. and C.S. performed light microscopy analysis. D.L. performed energy calculations. G.V.G. and M.H. recorded and analyzed E.M. data. M.L. and A.E. generated structure predictions. M.L. wrote the paper with input from all authors.

Data Availability

The density maps for the N-terminal region ("CryoEM structure of the human Nucleophosmin 1 core") and for the two selected 3D classes have been deposited in the EMDB (EMD-15,606). The refined atomic coordinates for the NPM1 core have been deposited in the PDB with (code 8AS5).

References

1. Boisvert FM, Van Koningsbruggen S, Navascués J, Lamond AI. 2007. The multifunctional nucleolus. Nat Rev Mol Cell Biol. 8:574–585.
2. Woods SJ, Hannan KM, Pearson RB, Hannan RD. 2015. The nucleolus as a fundamental regulator of the p53 response and a new target for cancer therapy. Biochim. Biophys. Acta—Gene Regul. Mech. 7:821–829.
3. Lafontaine DLJ, Riback JA, Bascetin R, Brangwynne CP. 2021. The nucleolus as a multiphase liquid condensate. Nat Rev Mol Cell Biol. 22:165–182.
4. Feric M, *et al.* 2016. Coexisting liquid phases underlie nucleolar subcompartments. Cell. 165:1686–1697.
5. Grisendi S, Mecucci C, Falini B, Pandolfi PP. 2006. Nucleophosmin and cancer. Nat Rev Cancer. 6:493–505.
6. Li F, *et al.* 2020. Epigenetic CRISPR screens identify Npm1 as a therapeutic vulnerability in non-small cell lung cancer. Cancer Res. 80:3556–3567.
7. Li Z, Hann SR. 2009. The Myc-nucleophosmin-ARF network: a complex web unveiled. Cell Cycle. 8:2703–2707.
8. Hyung HL, *et al.* 2007. Crystal structure of human nucleophosmin-core reveals plasticity of the pentamer-pentamer interface. Proteins: Struct, Funct, Genet. 69:672–678.
9. Mitrea DM, *et al.* 2018. Self-interaction of NPM1 modulates multiple mechanisms of liquid-liquid phase separation. Nat Commun. 9:842.
10. Grummitt CG, Townsley FM, Johnson CM, Warren AJ, Bycroft M. 2008. Structural consequences of nucleophosmin mutations in acute myeloid leukemia. J Biol Chem. 283:23326–23332.
11. Hingorani K, Szebeni A, Olson MOJ. 2000. Mapping the functional domains of nucleolar protein B23. J Biol Chem. 275:24451–24457.
12. Sakashita G, Kiyoi H, Naoe T, Urano T. 2018. Analysis of the oligomeric states of nucleophosmin using size exclusion chromatography. Sci Rep. 8:4008.
13. Mitrea DM, *et al.* 2016. Nucleophosmin integrates within the nucleolus via multi-modal interactions with proteins displaying R-rich linear motifs and rRNA. Elife. 5:e13571.
14. Hisaoka M, Nagata K, Okuwaki M. 2014. Intrinsically disordered regions of nucleophosmin/B23 regulate its RNA binding activity through their inter-and intra-molecular association. Nucleic Acids Res. 42:1180–1195.
15. Szebeni A, Olson MOJ. 1999. Nucleolar protein B23 has molecular chaperone activities. Protein Sci. 8:905–912.
16. Andersen JS, *et al.* 2005. Nucleolar proteome dynamics. Nature. 433:77–83.
17. Frottin F, *et al.* 2019. The nucleolus functions as a phase-separated protein quality control compartment. Science (80-.). 365:342–347.

18. Wang M, Bokros M, Theodoridis PR, Lee S. 2019. Nucleolar sequestration: remodeling nucleoli into amyloid bodies. Front Genet. 10:1179.
19. Marijan D, *et al.* 2019. Stress-specific aggregation of proteins in the amyloid bodies. FEBS Lett. 593:3162–3172.
20. Barucker C, *et al.* 2014. Nuclear translocation uncovers the amyloid peptide aβ42 as a regulator of gene transcription. J Biol Chem. 289:20182–20191.
21. Arosio P, *et al.* 2016. Kinetic analysis reveals the diversity of microscopic mechanisms through which molecular chaperones suppress amyloid formation. Nat Commun. 7:10948.
22. Huang L, *et al.* 2021. DAXX represents a new type of protein-folding enabler. Nature. 597:132–137.
23. Chen G, *et al.* 2017. Bri2 BRICHOS client specificity and chaperone activity are governed by assembly state. Nat Commun. 8:1356.
24. Lössl P, van de Waterbeemd M, Heck AJ. 2016. The diverse and expanding role of mass spectrometry in structural and molecular biology. EMBO J. 35:2634–2657.
25. Benesch JLP, Ruotolo BT. 2011. Mass spectrometry: come of age for structural and dynamical biology. Curr Opin Struct Biol. 21:641–649.
26. Benesch JLP. 2009. Collisional activation of protein complexes: picking up the pieces. J Am Soc Mass Spectrom. 20:341–348.
27. Landreh M, *et al.* 2017. Mass spectrometry captures structural intermediates in protein fiber self-assembly. Chem Commun. 53:3319–3322.
28. Abramsson ML, *et al.* 2021. Charge engineering reveals the roles of ionizable side chains in electrospray ionization mass spectrometry. JACS Au. 1:2385–2393.
29. Kaltashov I, Mohimen A. 2005. Estimates of protein surface areas in solution by electrospray ionization mass spectrometry. Anal Chem. 77:5370–5379.
30. Gallo A, *et al.* 2012. Structure of nucleophosmin DNA-binding domain and analysis of its complex with a G-quadruplex sequence from the c-MYC promoter. J Biol Chem. 287:26539–26548.
31. Jumper J, *et al.* 2021. Highly accurate protein structure prediction with AlphaFold. Nature. 596:583–589.
32. Zweckstetter M. 2021. NMR hawk-eyed view of AlphaFold2 structures. Protein Sci. 30:2333–2337.
33. Tsaban T, *et al.* 2022. Harnessing protein folding neural networks for peptide–protein docking. Nat Commun. 13:176.
34. Gibbs EB, Perrone B, Hassan A, Kümmerle R, Kriwacki R. 2020. NPM1 Exhibits structural and dynamic heterogeneity upon phase separation with the tumor suppressor ARF. Biophys J. 310:106646.
35. Mitrea DM, *et al.* 2014. Structural polymorphism in the N-terminal oligomerization domain of NPM1. Proc Natl Acad Sci U S A. 111:4466–4471.
36. Yu Y, *et al.* 2006. Nucleophosmin is essential for ribosomal protein L5 nuclear export. Mol Cell Biol. 26:3798–3809.
37. Liang CQ, Wang L, Luo YY, Li QQ, Li YM. 2021. Capturing protein droplets: label-free visualization and detection of protein liquid-liquid phase separation with an aggregation-induced emission fluorogen. Chem Commun. 57:3805–3808.
38. Ferrolino MC, Mitrea DM, Michael JR, Kriwacki RW. 2018. Compositional adaptability in NPM1-SURF6 scaffolding networks enabled by dynamic switching of phase separation mechanisms. Nat Commun. 9:5064.
39. Hochberg GKA, *et al.* 2014. The structured core domain of αb-crystallin can prevent amyloid fibrillation and associated toxicity. Proc Natl Acad Sci U S A. 111:E1562–E1670.
40. Mainz A, *et al.* 2015. The chaperone αb-crystallin uses different interfaces to capture an amorphous and an amyloid client. Nat Struct Mol Biol. 22:898–905.
41. Yang Y, *et al.* 2019. Cytoplasmic DAXX drives SQSTM1/p62 phase condensation to activate Nrf2-mediated stress response. Nat Commun. 10:3759.
42. Rapkin LM, *et al.* 2015. The histone chaperone DAXX maintains the structural organization of heterochromatin domains. Epigenetics Chromatin. 8:44.
43. Landreh M, *et al.* 2015. Controlling release, unfolding and dissociation of membrane protein complexes in the gas phase through collisional cooling. Chem Commun 51: 15582–15584.